Using Predictor Antennas for the Prediction of Small-scale Fading Provides an Order-of-Magnitude Improvement of Prediction Horizons

Joachim Björsell, Mikael Sternad
Signals and Systems, Uppsala University
PO Box 534, SE-751 21 Uppsala, Sweden
Email: {joachim.bjorsell,mikael.sternad}@angstrom.uu.se

Michael Grieger
AIRRAYS - Wireless Solutions Dresden, Germany
Email: michael.grieger@airrays.com

***Abstract*—Our aim is to investigate long range predictions (up to several wavelengths) of the small-scale fading of radio channels. The purpose is to enable advanced 5G downlink transmission schemes that require accurate channel state information at transmitters, such as massive MIMO and coherent joint transmission, for vehicular users.**

We here present a proof of concept for the recently introduced predictor antenna scheme which promises a significant increase in prediction horizon compared to conventional techniques. Predictor antennas utilize the exterior of moving vehicles by placing antenna arrays on top of their roofs. They are used to estimate the fading radio channels that are encountered later by the following antennas. The level of predictability is determined by the correlation between the channel measured at the predictor antenna and the channel that is later encountered by the following antennas when they move to that position. That correlation, and the resulting prediction errors, are assessed on a large set of measurement data sampled at vehicular velocities, at a carrier frequency of 2.53 GHz, from a multitude of urban fading environments. These represent a wide variety of propagation environments, including narrow and wide roads, intersections, dense urban environments and residential areas.

Using low-pass filtered predictor antenna measurements, the obtained average prediction Normalized Mean Squared Error (NMSE) is -11 dB for prediction horizons of 0.25 wavelengths and -8.5 dB for horizons of 3 wavelengths. This represents an order of magnitude increase of the prediction horizons as compared to time-series prediction that typically, in practice, fails to work for prediction beyond 0.3 wavelengths in space. As a result, we have a tool that enables advanced 5G transmit schemes for vehicular users and vehicle-to-infrastructure links.

I. Introduction

Areas of strong current interest for 5G are communication to vehicles for infotainment systems, local relay nodes [1] and traffic safety information using infrastructure-to-vehicle links.

Use of adaptive transmission techniques that require Channel State Information at the Transmitter (CSIT) could lower the cost and improve the quality of high-bandwidth and low latency links to vehicular users. Transmit schemes that require CSIT include fast link adaptation, maximum ratio and zero-forcing transmit beamforming, multi-user (massive) Multiple Input Multiple Output (MIMO) transmission, coherent Joint Transmission Coordinated MultiPoint (JT-CoMP) and distributed MIMO. However, the required CSIT will always be outdated for mobile users due to various time delays, which reduce performance [2], [3].

A. Prediction of outdated channels

This problem can be alleviated by using prediction estimates of the channels. Due to the small-scale fading, the phases and amplitudes of radio channels vary in space over a small fraction of a wavelength. The outdating problem therefore grows more severe at higher vehicle speeds and at shorter wavelengths. A required prediction horizon of L seconds (due to the transmission control delays) is equivalent to a prediction over space expressed in terms of carrier wavelengths:

$$Lf_d = \frac{Lv}{\lambda} = \frac{Lvf_c}{c_0} \quad \text{[wavelengths]} \ , \tag{1}$$

where f_d is the maximal Doppler frequency in Hz, v is the vehicle velocity in m/s, λ is the carrier wavelength in m, c_0 is the speed of light and f_c is the carrier frequency.

For example, a 5 ms prediction horizon at $f_c = 2.68$ GHz is $0.62\,\lambda$ at $v = 13.88$ m/s (50 km/h) and $1.24\,\lambda$ at $v = 27.77$ m/s (100 km/h). At pedestrian 5 km/h, it is only $0.062\,\lambda$.

The small-scale fading can be predicted based on noisy past channel estimates [4]–[6]. The best results are obtained by using Kalman predictors [7]. However, in practice, such predictors can rarely provide adequate performance for real channel measurements under realistic conditions for prediction horizons longer than 0.3 wavelengths [5], [7]. (Super-resolution techniques that assume sinusoidal channel variations will fail in practice.) This limits the use of channel prediction at vehicular velocities for carriers above 1 GHz in present 4G systems, where the control delays are 5 ms. With JT-CoMP, delays would be even longer.

One way to alleviate this problem would be to redesign the systems that are to be used below 6 GHz to reduce control loop latencies. Link adaptation performance for Rayleigh fading channels is illustrated in [8], [9] for latencies of 1-2 ms. Such designs are now of interest for low-latency 5G transmission. However, even with a transmission control delay of 1-2 ms, the required prediction horizon for higher vehicular velocities will still be longer than the at present predictable 0.3 wavelengths in space.

978-1-5090-1525-2/17/$31.00 ©2017 IEEE

B. Predictor antennas

Channel prediction is a hard problem, but additional measurements may be of help. Assuming a static surrounding, the electromagnetic field forms a standing wave pattern, and the vehicle moves through this pattern. An antenna on the roof of the vehicle senses this wave pattern and pilot-based channel estimation can be used to estimate it. If an antenna is placed in front of the ones of interest on the roof of the vehicle, it would sample the wavefield in advance. Its estimated channel could be used as predictor for the channels to be experienced by the rearward antennas when they reach this position.

On vehicles, we might use a linear array with antennas placed in the forward-backward direction, as illustrated by Fig. 1. Each antenna of the array could then be used to generate prediction estimates for the ones behind it.

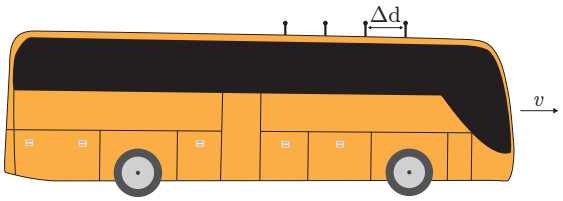

Fig. 1. Multiple antennas, where the one in front may act as predictor antenna.

Consider a simple case with two antennas on the roof. The channels constitute time-varying complex scalar gains for Orthogonal Frequency Division Multiplexing (OFDM) subcarriers. The front antenna channel $h_p(t)$ would then be of use for predicting the channel $h_m(t)$ at the rearward main antenna. The predictor is in the simplest case just a scaled and appropriately delayed filter estimate of h_p:

$$\hat{h}_m(t+L|t) = a\hat{h}_p(t+L-\Delta t|t+L-\Delta t)\ . \qquad (2)$$

Here, a is a complex-valued scalar gain, L is the required prediction horizon, and $\Delta t = \Delta d/v$, where Δd is the antenna separation and v is the vehicle velocity. Prediction horizons $L \leq \Delta t$ can be accommodated without extrapolating $\hat{h}_p$. A smoothing estimate $\hat{h}_p(t+L-\Delta t|t)$ could be used in (2) to increase performance at the price of higher computational complexity. The optimal adjustment of the gain a with noisy measurements will be discussed below in Section II.

The predictor antenna concept outlined above was first proposed in [10] and a similar approach was also proposed in [11]. It has been assessed experimentally based on two dedicated measurement campaigns in Dresden, Germany. The first measurements, reported in [10], were a preliminary pilot study that used two dipole antennas on the roof of a van. The second measurement campaign gave much better antenna correlation by using two monopole antennas and a flat, uncluttered vehicle roof [12]. Compensation of antenna coupling was in [12] found useful for closely-spaced antennas. However, these measurements were both performed at only two locations in an urban environment. The promising results could have been caused by a lucky accident of a propagation environment that was unusually simple to predict.

C. Summary of results

We here evaluate the results from a third, much more extensive, measurement campaign. It used improved equipment with four monopole antennas on a flat vehicle roof with various antenna spacings. Uplink measurements at 2.53 GHz ($\lambda = 11.94$ cm) at 90 subcarriers were received by multiple base stations of the TU Dresden 4G test-bed from a vehicle moving through central Dresden. The measurements and the signal processing are described later in Sections III and IV.

The results, to be described in more detail in Section V, are summarized by Fig. 2 which is based on all the used measurement locations. The over-all mean of the prediction Normalized Mean Squared Error (NMSE), its mode (peak location of the pdf) and the 25th and 75th percentiles are shown. The prediction horizon here equals the antenna spacing, $L = \Delta t = \Delta d/v$, using different antenna distances Δd. We also compare to the predictability when using Kalman prediction.

These new results are consistent with those reported in [12]. The mean NMSE obtained with prediction antennas is between -11 dB and -9 dB and it deteriorates only weakly with increasing prediction horizons up to 3 wavelengths. This represents an order-of-magnitude increase of the feasible horizon as compared to Kalman prediction that extrapolates past measurements. A majority of NMSE values are within a few dB of the mean NMSE. This prediction accuracy is sufficient for single-antenna link adaptation [8], [13] at moderate rates and for maximum ratio beamforming [14].

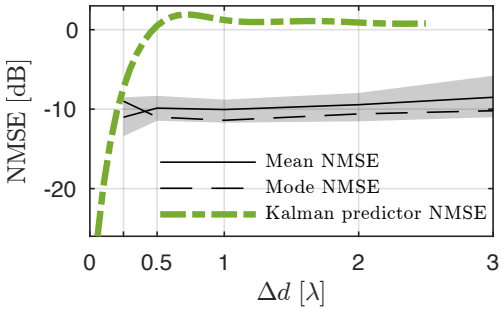

Fig. 2. Mean (solid) and mode (dashed) of the estimated prediction NMSE for a prediction antenna that uses low-pass filtered channel measurements. Results summarize the statistics from a large number of positions in an urban environment, as a function of the antenna distance Δd in wavelengths, which also here represents the prediction horizon. The gray marked area lies between the 25th and 75th percentiles. An example of a typical NMSE obtained by Kalman extrapolation of past measurements is shown for comparison. An AR model of order 6 for Rayleigh fading statistics is used here.

II. Predictor Antenna Performance Model

For two antennas, we may define $a_t(t+L)$ as the true but unknown fraction between the main channel h_m and a noise-free measurement of the predictor antenna channel h_p at the same position in space:

$$h_m(t+L) = a_t(t+L)h_p(t+L-\Delta t), \qquad (3)$$

where Δt was defined in (2). The time-varying complex scalar $a_t(t+L)$ would constitute the ideal predictor coefficient.

We here substitute $a_t(t+L)$ by a piecewise constant value a that is to be adjusted based on the second order statistics of the channels. We furthermore utilize a filter estimate $\hat{h}_p$ of h_p. This leads to the expression (2) for the predictor. We will now first assume that $\hat{h}_p = h_p$, and then in the next subsection model deviations by additive noise terms.

Assuming a perfect measurement of the predictor antenna channel h_p, it can be shown that the choice

$$a = b\frac{\sigma_m}{\sigma_p}, \tag{4}$$

minimizes the prediction Mean Squared Error (MSE)

$$\text{MSE} = \text{E}[|h_m(t+L) - a\hat{h}_p(t+L-\Delta t)|^2]. \tag{5}$$

In (4), $\sigma_m = \sqrt{\text{E}[|h_m|^2]}$ and $\sigma_p = \sqrt{\text{E}[|h_p|^2]}$ may be unequal since different transmitters/receivers are used. Furthermore, $b \in [-1, 1]$ is the normalized value of the channel correlation c at delay Δt such that

$$R_{h_m h_p}(\Delta t) = \text{E}[h_m(t)h_p^*(t-\Delta t)] = c = b\sigma_m\sigma_p. \tag{6}$$

By expanding (5) and applying (4) and (6), we obtain the theoretical prediction NMSE when $\hat{h}_p = h_p$, for a physical correlation b between the channels at the two antennas, as

$$\text{NMSE}_T = \frac{\text{MSE}}{\sigma_m^2} = 1 - |b|^2. \tag{7}$$

This limit of attainable performance as a function of $|b|$, based on (7), is shown in the left-hand part of Fig. 3.

With straight-line movement through a stationary wavefield, we should have $|b| = 1$. In reality, $|b| < 1$ for various reasons: Disturbance of the wavefield due to the moving vehicle itself, reflections and scattering via nearby moving vehicles, and also vibrations, lateral motion and curved motion of the vehicle. The last effects will cause lateral displacements of the antenna trajectories, that cause decorrelation.

A. Effects of measurement noise

We now model our measurements of the main antenna channel and of the predictor antenna channel as noisy signals $y_m(t)$ and $y_p(t)$ with $\text{E}[|y_m|^2] = \sigma_{y_m}^2$ and $\text{E}[|y_p|^2] = \sigma_{y_p}^2$,

$$y_m(t) = h_m(t) + e_m(t), \tag{8}$$
$$y_p(t) = h_p(t) + e_p(t), \tag{9}$$

where $e_m(t)$ and $e_p(t)$ are assumed zero mean, uncorrelated with the channels and mutually uncorrelated, so $\text{E}[e_m(t)e_p^*(t-\tau)] = 0$. These simple models, with unit gains between y and h, are appropriate for the pilot-based channel estimates that were produced from our measurements. They also remain approximately valid after applying the linear low-pass filter described in Section IV, since the low-pass filters have gain 1 in their passband.

It is furthermore assumed here, but not necessary, that $e_m(t)$ and $e_p(t)$ have equal variance σ_e^2, which gives the Signal-to-Noise Ratio (SNR) of the channel measurements

$$\gamma_m = \sigma_m^2/\sigma_e^2, \tag{10}$$
$$\gamma_p = \sigma_p^2/\sigma_e^2. \tag{11}$$

If we are to predict the true channel $h_m(t+L)$ from the noisy measurements of the predictor antenna channel $\hat{h}_p(t+L-\Delta t|t+L-\Delta t) = y_p(t+L-\Delta t)$, then the noise $e_p(t)$ at the predictor antenna will reduce the predictability. By minimizing the MSE

$$\text{E}[|h_m(t+L) - a_h y_p(t+L-\Delta t)|^2], \tag{12}$$

the optimal constant prediction coefficient a_h is obtained as

$$a_h = \frac{c}{\sigma_{y_p}^2} = \frac{b\sigma_m\sigma_p}{\sigma_p^2 + \sigma_e^2} = b\frac{\sqrt{\gamma_m\gamma_p}}{1+\gamma_p}, \tag{13}$$

which results in the SNR-dependent theoretical NMSE

$$\text{NMSE} = 1 - |b_h|^2 = 1 - |b|^2\frac{\gamma_p}{(1+\gamma_p)}, \tag{14}$$

where

$$b_h = \frac{c}{\sigma_{y_p}\sigma_m}, \tag{15}$$

is the normalized correlation between the main antenna channel h_m and the noisy predictor antenna channel y_p.

The NMSE in (14) is plotted against the prediction antenna SNR γ_p in the right-hand part of Fig. 3 for different antenna correlations b.

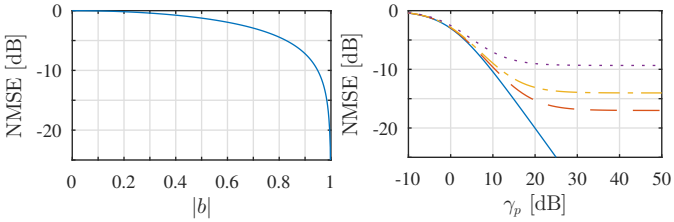

Fig. 3. The left-hand plot shows the theoretical NMSE for perfect measurements by (7), as a function of the magnitude $|b|$, of the normalized correlation between the channels by (6). The right-hand plot shows the theoretical NMSE as a function of the SNR of the predictor channel measurements, γ_p, by (14). The different lines show the relation for the physical correlations, $b = 1$, solid line (——), $b = 0.99$, dashed line (– –), $b = 0.98$, dashed-dotted line (–·–) and $b = 0.94$, dotted line (·····).

B. The NMSE expressed in measurable quantities

Our aim is to evaluate the effectiveness of predicting the main antenna channel $h_m(t)$, but unfortunately $h_m(t)$ itself is unavailable. Only the noisy estimates $y_m(t)$ are available.

The theory above can be utilized to estimate the prediction NMSE also when the true main channel h_m is unknown. From the assumptions on $e_m(t)$ and $e_p(t)$ we obtain

$$\begin{aligned} c &= \text{E}[h_m(t)h_p^*(t-\Delta t)] = \text{E}[h_m(t)y_p^*(t-\Delta t)] \\ &= \text{E}[y_m(t)y_p^*(t-\Delta t)], \end{aligned} \tag{16}$$

and

$$\sigma_m^2 = \sigma_{y_m}^2 - \sigma_e^2, \tag{17}$$

which both can be used in (15) to obtain an estimate of b_h which in turn gives the NMSE by (14).

The attainable NMSE will here be evaluated by using (15) and (14) , using data-based point estimates of the noise power σ_e^2, the correlation c and the variances $\sigma_{y_p}^2$ and $\sigma_{y_m}^2$.

III. Measurements

The measurements were obtained by driving in downtown Dresden, Germany, depicted in Fig. 4, with velocities between 1 km/h to 50 km/h. The physical layer parameters that were used are in close compliance with the 3GPP/LTE standard. Since the focus of the current paper is on channel estimation and prediction, only the demodulation reference symbols are evaluated. The channel was measured in the uplink direction using the demodulation reference symbols transmitted by the roof-mounted antennas on the vehicle.

A. Measurement equipment

The OFDM signals, transmitted at 2.53 GHz with 5.4 MHz bandwidth, were simultaneously received and recorded at up to 16 Base Stations (BSs) located on five sites with up to six-fold sectorization. Each BS was equipped with a two element, cross-polarized KATHREIN 80010541 antenna which has $58°$ horizontal and $6.1°$ vertical half power beam width. Time and frequency synchronization of the BSs was done through GPS fed reference normals.

The linear array of four monopole antennas was positioned on the roof of a Volkswagen T4 van in a straight line in the forward-backward direction as shown in Fig. 5. Different antenna distances $\Delta d = \{0.25, 0.5, 1, 2, 3\}\,\lambda$ were used during different measurement campaigns. A metal sheet was used below the antennas in order to have an idealized local surrounding that was independent of the particular type of vehicle.

At the BSs, snapshots of 640 ms duration of the digital received base band signal were stored after down-conversion, analogue-digital conversion, sample rate conversion, and filtering. One snapshot was captured about every minute. All other receiver algorithms such as synchronization, carrier frequency offset compensation, OFDM demodulation and channel estimation were applied offline.

The reference signals from the four antennas of the vehicle used separate regularly spaced sets of 15 kHz subcarriers, with reference signals from each antenna placed on every 4:th subcarrier. With a symbol estimation period of 0.5 ms, this resulted in 1280 channel estimates over time on 90 subcarriers, each separated by 60 kHz, per snapshot and antenna.

B. Channel measurement quality and selection of data set

The measurements were affected by hardware impairments such as gain imbalances on different transmit/receiver paths and phase noise. Thus, a compound channel (similar to a system used in the real world) including hardware effects, antenna effects, and the wireless channel was measured.

The transmitters of the vehicle antennas were equipped with independent local oscillators which were not fully frequency synchronized. This caused frequency offsets between the different antenna branches. All resulting effects of this have been corrected with high precision by adding a linearly increasing/decreasing phase shift to the channel estimate time

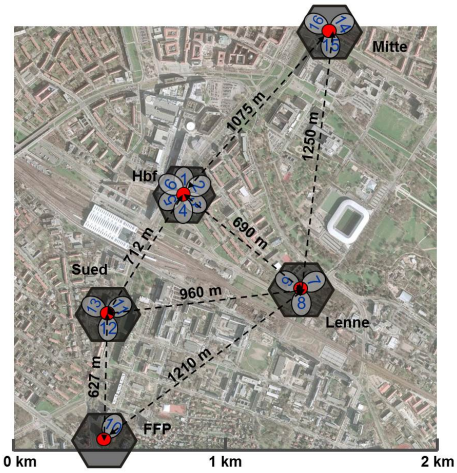

Fig. 4. Map over the measurement area in Dresden with base station locations and directions marked.

Fig. 5. The Volkswagen T4 van on the left hand side and zoomed into the antenna array on the roof on the right hand side.

series of the second, third and fourth antenna to maximize the correlation over time with the first antenna.[1]

Three subsets of data are removed from the study performed here. The first of these contains distortion of unknown cause, that generates periodical spikes in the Doppler spectra. Second, measurements at vehicle velocity $v = 0$ are not used. Third, only data sets with at least 350 time samples overlapping in space, between the predictor channel and main channel, is used. In other words, only measurements sets where at least 350 time samples are sampled after the main antenna has reached the initial position of the predictor antenna. The resulting numbers of available, relevant and utilized measurements (transmit antenna-base station pairs) are shown in Table I.

After the selection process of the measurements, approximately 650 million subcarrier channel estimates (1280 time samples x 90 subcarriers per measurement) are used in the results in Section V. They represent a wide variety of propagation environments, including narrow and wide roads, intersections, dense urban environments and residential areas.

IV. Signal Processing

A. Low-pass filtering

The SNR of the utilized measurement series $y_m(t)$ and $y_p(t)$ varies between 0 dB and 30 dB. The channel measurements

[1] In a non-experimental implementation, no relative frequency offsets would occur, since the antennas would use a common clock reference.

TABLE I
NUMBER OF MEASUREMENTS FOR DIFFERENT ANTENNA DISTANCES Δd

Campaign	Available	Relevant†	Used*	Percentage used
$\Delta d = 0.25\,\lambda$	459	115	115	25%
$\Delta d = 0.5\,\lambda$	490	305	305	62%
$\Delta d = 1\,\lambda$	519	355	355	68%
$\Delta d = 2\,\lambda$	577	358	348	60%
$\Delta d = 3\,\lambda$	543	346	322	59%

† Measurements for vehicle velocities $v > 0$ and with the variance of the high-frequency tails of the Doppler spectra less the 0.5 dB.
* Measurements that fulfill † and with velocities so that at least 350 time samples are sampled after the main antenna has reached the initial position of the predictor antenna.

are filtered to suppress the noise and we investigate the effect of the filtering on the prediction performance.

The noise filtering is here performed by applying a linear phase low-pass Finite Impulse Response (FIR) filter to the time-domain signals. The FIR filter is of order 140 and its passband is designed individually for each measurement to be somewhat wider than the Doppler spectrum of the signal.

An example is illustrated in Fig. 6 where a typical Doppler spectrum of an unfiltered channel measurement and the corresponding low-pass filtered channel measurements can be seen.

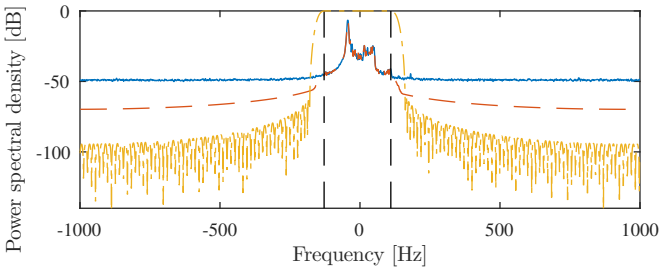

Fig. 6. Doppler spectrum, of a channel measurement (——), the low-pass filtered channel measurement (– –) (including the effect of time-windowing from using 1280 samples) and the frequency response of the FIR-filter (– · –) with the passband limits shown by the vertical lines (– –).

B. Noise estimation

The noise power σ_e^2, which is used in (17) for use in the NMSE estimation, is estimated from the Doppler spectra of each measurement set. The measurement noise is assumed to be white and uncorrelated over frequency. The assumption is based on the flat high-frequency tails in the Doppler spectra, as in Figure 6, and the lack of correlation, both in time and frequency, for high-pass filtered measurements (containing only noise). Under this assumption it is possible to estimate the measurement noise power from the high-frequency tails of the Doppler spectra. The same noise power is also used to estimate the SNR by

$$\hat{\gamma} = \frac{\hat{\sigma}_y^2}{\hat{\sigma}_e^2} - 1, \tag{18}$$

where $\hat{\sigma}_y^2$ is the estimated power of the noisy channel and $\hat{\sigma_e^2}$ is the estimated noise power.

By applying the low-pass FIR filter to artificially generated measurement noise, it is possible to estimate the noise power in the low-pass filtered channel measurements.

C. Estimation of the prediction NMSE

Denote the row vectors of N time samples at one subcarrier of $y_p(t)$ and $y_m(t)$ by $\mathbf{y}_p$ and $\mathbf{y}_m$. From these, the variance $\sigma_{y_p}^2$ and σ_m^2 by (17) are estimate by

$$\hat{\sigma}_{y_p}^2 = \mathbf{y}_p \mathbf{y}_p^*/N, \tag{19}$$

$$\hat{\sigma}_m^2 = \mathbf{y}_m \mathbf{y}_m^*/N - \hat{\sigma}_e^2. \tag{20}$$

For unfiltered measurements, $\hat{\sigma}_e^2$ is calculated from the high-frequency tails of the Doppler spectra. For low-pass filtered measurements, we use

$$\hat{\sigma}_e^2 = \frac{1}{NJ} \sum_{t=1}^{N} \sum_{j=1}^{J} \tilde{e}_j(t) \tilde{e}_j^*(t), \tag{21}$$

where $\tilde{e}_j(t)$ is the low-pass filtered, artificially generated noise at time t and subcarrier j.

The correlation c in (15) is estimated by

$$\hat{c} = \arg\max_{\hat{\mathbf{c}}} |\hat{\mathbf{c}}|, \tag{22}$$

where $\hat{\mathbf{c}}$ is a vector containing the correlations between $\mathbf{y}_p$ and $\mathbf{y}_m$ for all possible time-lags $\tau \in [-N+1, N-1]$, calculated by

$$\hat{\mathbf{c}} = \mathcal{F}^{-1}[\mathcal{F}(\mathbf{y}_m) \odot \mathcal{F}(\mathbf{y}_p)^*]. \tag{23}$$

Here, $\odot$ is element-wise multiplication and $\mathcal{F}$ and $\mathcal{F}^{-1}$ are the Fourier respectively the inverse Fourier operators.[2]

The NMSE is then estimated per subcarrier from (14) and (15) by using the estimates given by (19)-(22).

Less than 0.1 % of the resulting NMSE estimates become negative due to estimation errors. These estimates are not included in the results.

Note that this estimate of the NMSE is based on current channel statistics, and is therefore somewhat optimistic: We estimate the attainable NMSE from a complete time series at a given location. In a real situation, the adjustment of the predictor would be based on a previous time window, and could therefore be somewhat outdated.

V. RESULTS

The aggregated results for the estimated NMSE for all measurements is summarized by Fig. 2 in Section I. The prediction performance can be further analyzed for each antenna distance. Each measurement (location and transmit antenna-BS pair) is here analyzed individually.

[2]Before performing (19)-(22), the time series are adjusted to only contain undistorted samples so that each sample in $\mathbf{y}_p$ corresponds to a sample in $\mathbf{y}_m$ from approximately the same position in space. The first 140 samples are removed from the low-pass filtered channel measurements as they contain a FIR filtering transient. Then, the last $\Omega = 2000\Delta d/\hat{v}$ time samples from the predictor antenna measurements and the first Ω samples from the main antenna measurements are removed as these samples lack matching samples (sampled at the same location in space) in the time series of the other antenna. The effects of estimation errors in $\hat{v}$ are current under investigation.

A. The prediction performance and its SNR dependence

In Fig. 7 a scatter plot is shown of the relation between the estimated NMSE (14) and SNR of the predictor antenna (18). Results are for both the unfiltered (marked by yellow dots •) and the low-pass filtered (marked by black dots •) channel measurements with antenna separation (and prediction horizon) $\Delta d = 0.5\,\lambda$. The figure is complemented by a distribution plot, of the NMSE for the same data. To increase the readability of the scatter plot, the NMSE is there averaged over all subcarriers from the same measurements burst. Four lines indicate the theoretical relationship (14) between NMSE and SNR when $|b| = \{0.94, 0.96, 0.98, 0.99\}$.

The improved SNR, as a results of the low-pass filtering, can be seen by the right shifted cluster of black dots as compared to yellow ones in the scatter plot. It is further emphasized by the SNR distribution in Fig. 8. The wide interval of SNR of the channel measurements provides information about the relation between SNR and NMSE and the relevance of the model (14). A majority of the channel measurements in the scatter plot are around the indicated theoretical lines. However, as the underlying correlation $|b|$ is unknown, we have no direct way of verifying the theory.

The correlation b evidently varies quite substantially in different environments. We are analyzing the causes of these variations, but the results are not yet available.

The NMSE distributions on the right-hand side in Fig. 7 are unimodal. The SNR improvements by low-pass filtering reduces the NMSE by 2-3 dB on average, yielding a mean and mode NMSE of approximately -10 dB for the low-pass filtered channel measurements.

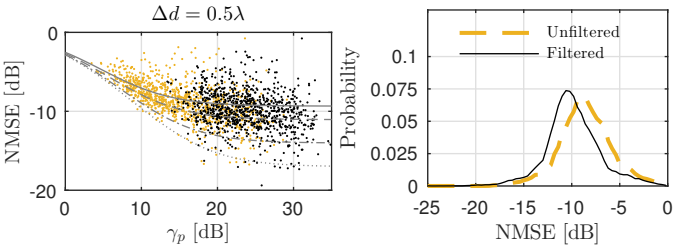

Fig. 7. Prediction performance of the predictor antenna using unfiltered (•) and low-pass filtered (•) channel measurements with antenna separation and prediction horizon $\Delta d = 0.5\,\lambda$. To the left is a scatter plot of the estimated NMSE, averaged over all subcarriers, versus the SNR of $\hat{h}_p = y_p$. Lines indicate the theoretical NMSE for a given SNR in the channel estimates by (14) for $|b| = 0.94$ (——), $|b| = 0.96$ (– –), $|b| = 0.98$ (– · –) and $|b| = 0.99$ (·····). To the right is the PDF of the NMSE for each subcarrier of the data shown in the scatter plot.

B. Prediction performance for varying prediction horizons and antenna separations

The scatter plots and the NMSE distributions for the other measurement campaigns with antenna distances (and prediction horizons) $\Delta d = \{0.25, 1, 2, 3\}\,\lambda$ are shown in detail in Fig. 9, with summary in Fig. 2. The PDF of the NMSE for $\Delta d = 0.25\,\lambda$ has a different shape as compared to the other antenna distances: A larger part of the predictions are located

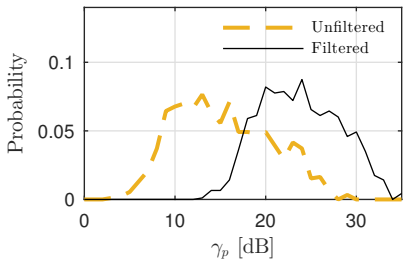

Fig. 8. Distribution of the SNR of the predictor antenna for the unfiltered (– –) and low-pass filtered (——) channel measurements, with antenna separation $\Delta d = 0.5\,\lambda$, from the measurements shown in the scatter plot in Fig. 7.

at the lower part of the NMSE distribution, below -14 dB, while the mode (location of the peak) is higher. This could be due to mutual electromagnetic coupling between the closely spaced antennas, as discussed in [12]. For the other antenna distances the NMSE mode for the low-pass filtered channel measurements is located at approximately -10 dB to -11 dB, the same as for $\Delta d = 0.5\,\lambda$.

Although the mode of the NMSE is fairly constant for $\Delta d > 0.25\,\lambda$, an increasing fraction of bad predictions (> -7 dB) appear at longer antenna distances/prediction horizons. This increases the average NMSE. The unknown cause of these bad prediction events is greatly correlated with lower velocities: They practically disappear at higher speeds. This is illustrated in Fig. 9 where the NMSE distribution is shown for filtered measurements at vehicle velocities above the empirically found thresholds 21 km/h for $\Delta d = 2\,\lambda$ and 25 km/h for $\Delta d = 3\,\lambda$.

VI. Discussion and Conclusion

We have investigated the use of predictor antennas on a large set of measurement data, obtained for moving vehicles in an urban environment with four antennas on the roof. The resulting prediction NMSEs of OFDM channels was found to typically be in the range -12 dB to -9 dB. Prediction with a NMSE above -7 dB was extremely rare at higher velocities, above 20-25 km/h, and there are no signs of reduced prediction performance for higher velocities than 50 km/h.

A subset of measurements at low velocity resulted in bad prediction performance. Such problems could be handled by combining predictor antenna estimates with Wiener or Kalman predictions that use the main antenna signals. These work well at low velocities (short prediction horizons in space by (1)).

We have used simple low-pass filtering for noise suppression, which could be substituted by more advanced filters or possibly by lower order filters. The scatter plots in Section V combined with the theory of Section II-A indicate that most of the performance gains from noise filtering comes from increasing the SNR to approximately 20 dB. The low-pass filters succeed in this in a majority of the cases. Thus, the utilized simple low-pass filter could very well be a fully functional, low-complexity, pre-processing algorithm to a prediction antenna system that has a high pilot sampling rate.

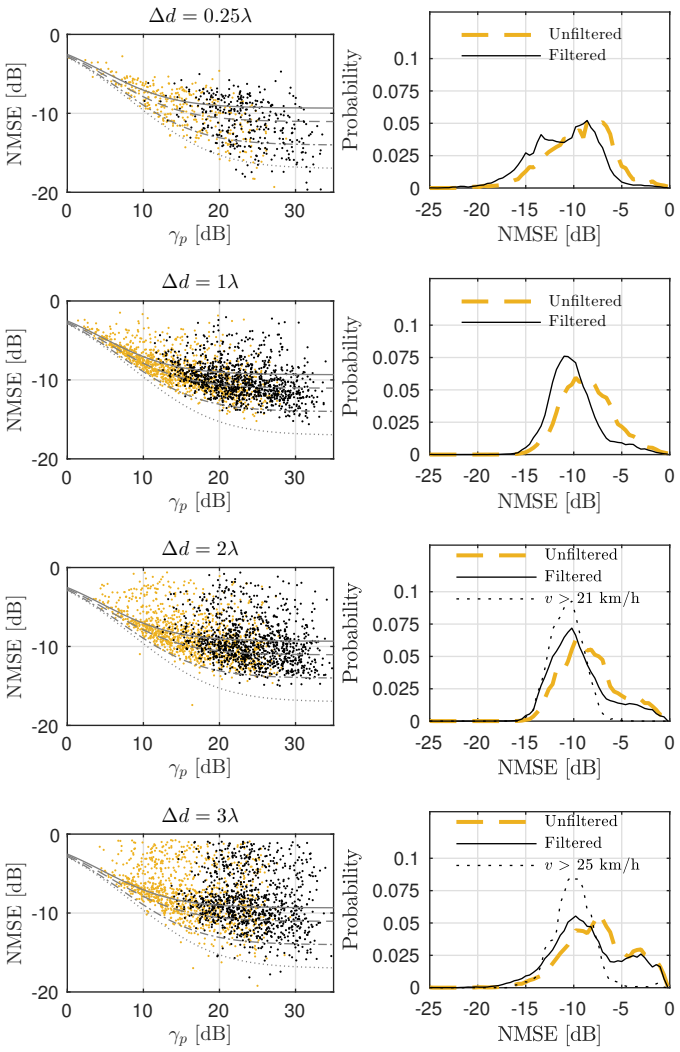

Fig. 9. Prediction performance of the predictor antenna using unfiltered (●) and low-pass filtered (●) channel measurements with antenna separation and prediction horizon $\Delta d = 0.25\,\lambda$ (first row), $\Delta d = 1\,\lambda$ (second row), $\Delta d = 2\,\lambda$ (third row) and $\Delta d = 3\,\lambda$ (fourth row). To the left is a scatter plot of the estimated NMSE for all utilized measurements, averaged over all subcarriers, versus the SNR of $\hat{h}_p = y_p$. Lines indicate the theoretical NMSE for a given SNR in the channel estimates (14) for $|b| = 0.94$ (——), $|b| = 0.96$ (— —), $|b| = 0.98$ (— - —) and $|b| = 0.99$ (·····). To the right is the PDF of the NMSE of the data shown in the scatter plot.

The conclusions are that the predictor antennas shows promising results in a large variety of fading environments with a realistic setup. In particular, it enables precise maximum ratio transmit beamforming [14]. It is here of interest that beamforming that uses many antenna elements becomes less sensitive with respect to estimation errors of each channel [15]. The NMSE of a maximum ratio beamforming combination of N antenna channels that have equal average channel power and NMSE will be a factor $1/N$ of the individual channel NMSEs.

As illustrated in [16], the ability to use coherent downlink transmissions from massive antenna arrays increases both the power efficiency and the spectral efficiency when serving connected vehicles. This is of significant importance for operators, as a rapidly increasing number of connected vehicles would otherwise have to be served with less efficient diversity-based transmission schemes.

Acknowledgments

We thank the 5G Lab at TU Dresden (Prof. Gerhard Fettweis) for providing the test-bed hardware and software that was used for these measurements. The data analysis work was partially supported by Orange Labs, under contract F03131.

References

[1] Y. Sui, J. Vihrälä, A. Papadogiannis, M. Sternad, W. Yang and T. Svensson, "Moving cells: A promising solution to boost performance for vehicular users," *IEEE Comm. Mag.* , vol. 51, no. 6, June 2013, pp. 62-68.

[2] S. Wagner, R. Couillet, M. Debbah, and D. Slock, "Large system analysis of linear precoding in correlated MISO broadcast channels under limited feedback." *IEEE Trans. on Inf. Theory*, vol. 58, no. 7, pp. 4509-4537, 2012.

[3] L. Thiele, M. Olbrich, M. Kurras, and B. Matthiesen, "Channel aging effects in CoMP transmission: Gains from linear channel prediction," in *45th Asilomar Conf. on Signals, Systems and Computers*, (Pacific Grove, USA), Nov. 2011.

[4] T. Ekman, A. Ahlén and M. Sternad, "Unbiased power prediction on Rayleigh fading channels," *IEEE Vehicular Techn. Conf. VTC2002-Fall*, Vancouver, Canada, Sept. 2002.

[5] T. Ekman, *Prediction of Mobile Radio Channels: Modeling and Design.* Ph.D. Thesis, Signals and Systems, Uppsala Univ., 2002. Available: www.signal.uu.se/Publications/pdf/a023.pdf

[6] A. Duel-Hallen, "Fading channel prediction for mobile radio adaptive transmission systems," *Proc. of the IEEE*, vol. 95, no. 12, pp. 2299-2313, Dec. 2007.

[7] D. Aronsson, *Channel Estimation and Prediction for MIMO OFDM Systems - Key Design and Performance Aspects of Kalman-based Algorithms.* Ph.D. Thesis, Signals and Systems, Uppsala University, March 2011. www.signal.uu.se/Publications/pdf/a112.pdf

[8] M. Sternad, S. Falahati, T. Svensson and D. Aronsson, "Adaptive TDMA/OFDMA for wide-area coverage and vehicular velocities," *IST Summit*, Dresden, June 19-23, 2005.

[9] M. Sternad, T. Svensson, T. Ottosson, A. Ahlén, A. Svensson and A. Brunstrom, "Towards systems beyond 3G based on adaptive OFDMA transmission," *Proceedings of the IEEE*, vol. 95, no. 12, pp. 2432-2455, Dec. 2007.

[10] M. Sternad, M. Grieger, R. Apelfröjd, T. Svensson, D. Aronsson and A. Belen Martinez, "Using "predictor antennas" for long-range prediction of fast fading moving relays," *IEEE Wireless Communications and Networking Conference (WCNC)*, Paris, April 2012.

[11] D.-T. Phan-Huy and M. Hélard, "Large MISO beamforming for high speed vehicles using separate receive & training antennas," *IEEE Int. Symposium on Wireless Vehicular Communication*, June 2013.

[12] N. Jamaly, R. Apelfröjd, A. Belen Martinez, M. Grieger, T. Svensson, M. Sternad and G. Fettweis, "Analysis and measurement of multiple antenna systems for fading channel prediction in moving relays," *European Conference on Antennas and Propagation, (EuCAP 2014)*, April 6-11 2014, Hauge, The Netherlands.

[13] S. Falahati, A. Svensson, M. Sternad and T. Ekman, "Adaptive modulation systems for predicted wireless channels," *IEEE Trans. on Communications*, vol. 52, pp. 307-316, Feb. 2004.

[14] D-T Phan-Huy, M. Sternad and T. Svensson, "Making 5G adaptive antennas work for very fast moving vehicles," *IEEE Intelligent Transportation Systems Magazine*, Summer, 2015, pp. 71-84.

[15] E. Björnson, J. Hoydis, M. Kountouris and M. Debbah, "Massive MIMO systems with non-ideal hardware: Energy efficiency, estimation, and capacity limits," *IEEE Trans. on Information Theory*, vol. 60, no. 11, pp. 7112-7139, Nov. 2014.

[16] D.-T. Phan-Huy, M. Sternad, T. Svensson, W. Zirwas, B. Villeforceix, F. Karim and S.-E. El-Ayoubi, "5G on board: How many antennas do we need on connected cars?" *IEEE Globecom 2016 Workshop on 5G RAN Design*, Washington DC, Dec. 2016.